CrossMark
click for updates

Highly enhanced photocatalytic activity of WO₃ thin films loaded with Pt–Ag bimetallic alloy nanoparticles†

Pengyu Dong,[*a] Bairen Yang,[b] Chao Liu,[c] Fenghua Xu,[c] Xinguo Xi,[d] Guihua Hou[a] and Rong Shao[*d]

WO₃ thin films loaded with Pt–Ag bimetallic alloy nanoparticles were successfully synthesized by a three-step method involving the formation of a homogeneous precursor sol, spin coating as well as UV-light reduction, and calcination. Moreover, a systematic, comparative study of the microstructure, chemical environment and electrochemical characteristics of the as-prepared Pt/WO₃, Ag/WO₃, and Pt–Ag/WO₃ thin films was carried out. It was found that the Pt–Ag/WO₃ thin film exhibited a highly enhanced photocatalytic performance for the degradation of methylene blue solution compared with the pure WO₃, Pt/WO₃ and Ag/WO₃ thin films. Based on the experimental results and the energy-band diagrams, the transfer paths of photogenerated charges and the enhanced photocatalytic mechanism were proposed. It was suggested that the photogenerated electrons from the conduction band of WO₃ first transferred to Ag and then to Pt in the Pt–Ag/WO₃ sample during the photocatalytic process, promoting the efficient two-electron reduction of O₂ compared to in the Pt/WO₃ and Ag/WO₃ samples. In addition, this process prevented the oxidation of Ag in the Pt–Ag/WO₃ sample during the photodegradation process in air. Overall, this study provides a novel approach to design efficient photocatalysts decorated by bimetallic alloy nanoparticles.

1. Introduction

It is well-known that photocatalysis is a promising technology for the production of hydrogen energy and the purification of environmental pollutants. In the past decades, TiO₂, a traditional and typical photocatalyst, was widely and deeply investigated.[1,2] However, the wide band gap (3.2 eV) of TiO₂ photocatalyst greatly limits its further application, especially in applications that utilize visible light.

WO₃, a visible light-responsive photocatalyst, absorbs light at wavelengths up to 480 nm and has intriguing merits such as low cost, harmlessness, and stability in both acidic and oxidative conditions,[3–5] leading to extensive application prospects in the field of visible light-driven photocatalysts. However, researchers have to face the fact that the photocatalytic activity of pure WO₃ semiconductor without any suitable optimization is relatively low,[6] which can be attributed to the rapid recombination of photogenerated charges and the relatively positive conduction band (CB) edge (+0.5 V *vs.* normal hydrogen electrode (NHE) at pH = 0) of WO₃.[6,7]

Recently, the deposition of noble metals on the surface of WO₃ semiconductor has been proven to be an effective strategy for improving the photocatalytic activity of WO₃. Abe *et al.* demonstrated that the photocatalytic activity of WO₃ loaded with Pt nanoparticles was almost comparable to that of TiO₂ under UV light irradiation and much higher than that of N–TiO₂ under visible light irradiation for the decomposition of organic acetic acid.[8] Subsequently, other research groups supported the conclusion of Abe *et al.*[8] using various experimental approaches.[9–14] Our research group investigated the effect of carriers on the photocatalytic activity for purification of NO gas over Pt/WO₃ catalyst and found that Pt/WO₃–zeolite molecular sieves (carrier) exhibited the highest conversion efficiency.[15] The Pt/WO₃ photocatalyst exhibited high efficiency for both the decomposition of organic compounds and the purification of NOₓ. However, the high cost of Pt should not be ignored in photocatalytic applications. Apart from the noble metal Pt nanoparticles, Ag nanoparticles have been used to improve the

[a]*Key Laboratory for Advanced Technology in Environmental Protection of Jiangsu Province, Yancheng Institute of Technology, Yancheng, 224051, P. R. China. E-mail: dongpy11@gmail.com; Fax: +86-515-8829-8923; Tel: +86-515-8829-8923*

[b]*School of Environmental Science and Engineering, Yancheng Institute of Technology, Yancheng 224051, China*

[c]*School of Materials Engineering, Yancheng Institute of Technology, Yancheng, 224051, P. R. China*

[d]*Jiangsu Collaborative Innovation Center for Ecological Building Materials and Environmental Protection Equipments, Yancheng Institute of Technology, Yancheng 224051, China. E-mail: sr@ycit.cn*

† Electronic supplementary information (ESI) available: Details of electrochemical measurement, TEM images of Pt–Ag/WO₃ sample, the survey XPS spectra of as-prepared samples, UV-vis absorption spectra of MB solutions. See DOI: 10.1039/c6ra25272a

photocatalytic activity of WO_3 because of the low cost and surface plasmon resonance (SPR) effect of Ag nanoparticles. For example, Sun *et al.* found that an as-synthesized Ag/mesoporous WO_3 sample exhibited superior photocatalytic activity for the decomposition of a common air pollutant (*i.e.*, acetaldehyde) compared to mesoporous WO_3, Ag/commercial WO_3 and N–TiO_2 under visible-light irradiation.[16] Nevertheless, preventing the oxidation of surface Ag atoms in air atmosphere remains a great challenge.

It was reported that compared to the corresponding Pt or Ag monometallic catalysts, their combination resulted in an obvious synergistic effect and significantly enhanced the catalytic activity in the absence of light irradiation.[17–19] However, the utilization of Pt–Ag for enhancing photocatalytic activity has seldom been investigated. To some extent, a better photocatalytic activity might be expected if Pt and Ag were simultaneously used to modify WO_3, especially WO_3 thin films. This is because WO_3 thin film can be repeatedly used without a complicated recycling process, which is necessary for conventional powder photocatalysts, and is hardly lost during photocatalytic reaction.[11,20–28]

In this work, we fabricated WO_3 thin-film photocatalysts co-modified by Pt–Ag bimetallic alloy nanoparticles (Pt–Ag/WO_3) by simultaneously photo-depositing Pt and Ag precursor ions on a WO_3 thin film to address the shortages of monometals Pt and Ag. Based on a systematic, comparative study of the microstructure, chemical environment and electrochemical characteristics of the prepared Pt/WO_3, Ag/WO_3, and Pt–Ag/WO_3 thin films, the transfer paths of photo-generated charges and photocatalytic mechanism were proposed.

2. Experimental section

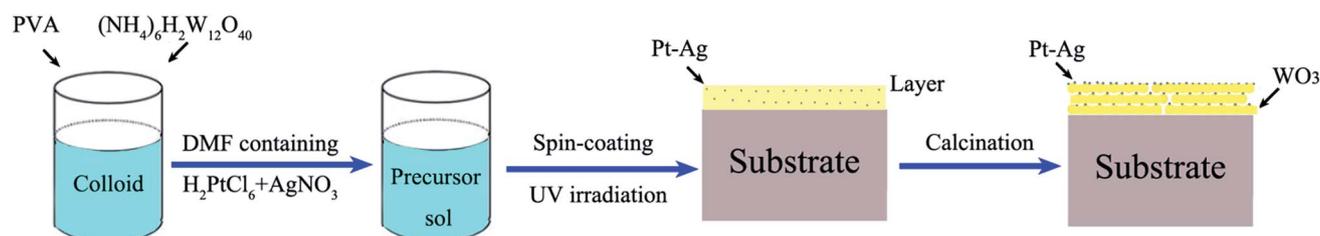### 2.1 Preparation of Pt–Ag/WO_3 thin film

The entire preparation process can be divided into three steps. First, the precursor sol was synthesized as follows: 3.45 μmol polyvinyl alcohol (PVA; average molecular weight: 129 710; polymerization degree: 1750) was dissolved in deionized water (60 mL) with stirring at 80 °C for 1 h in a water bath to form a colloid. Next, 0.6 mmol ammonium metatungstate ($(NH_4)_6H_2W_{12}O_{40}$, 99%) was added into the above colloid and stirred for 24 h to form a homogeneous precursor sol, which could remain stable for seven days. Second, a mixture of 0.5 mL of 10 mM H_2PtCl_6 and 0.5 mL of 10 mM $AgNO_3$ in *N,N*-dimethylformamide (DMF) solution was added into the above

precursor sol (2 mL) and mixed with stirring. Next, 3 mL of the precursor sol containing the H_2PtCl_6 and $AgNO_3$ solution was spin coated onto an indium-tin oxide (ITO) substrate with dimensions of 3 × 3 cm at a rate of 3000 rpm for 50 s using a spin coater and then dried at room temperature to form a precursor gel. Subsequently, the layer was illuminated with UV light (365 nm, 500 W) for 3 h so that the platinum and silver salts (H_2PtCl_6 and $AgNO_3$) were reduced from Pt^{4+} and Ag^+ to Pt^0–Ag^0. Finally, calcination was conducted in a drop-tube furnace at a heating rate of 1 °C min^{-1} for 5 h at 550 °C in N_2 atmosphere. The schematic illustration of the growth process is shown in Scheme 1.

For comparison purposes, a pure WO_3 thin film was prepared under the same conditions without adding H_2PtCl_6 and $AgNO_3$ in DMF solution and without the reduction process under UV light irradiation. A Pt/WO_3 thin film was prepared under the same conditions except that 0.5 mL of 10 mM H_2PtCl_6 in DMF solution was added instead of 0.5 mL of 10 mM H_2PtCl_6 and 0.5 mL of 10 mM $AgNO_3$. A Ag/WO_3 thin film was prepared under the same conditions except that 0.5 mL of 10 mM $AgNO_3$ in DMF solution was added instead of the mixture of H_2PtCl_6 and $AgNO_3$.

2.2 Characterization

Thermogravimetric and differential scanning calorimetric analyses (TG-DSC) were performed with a NETZSCH DSC 200 F3 instrument under N_2 flow. Measurements were conducted from room temperature to 600 °C at a heating rate of 10 °C min^{-1}. X-ray diffraction (XRD) experiments were carried out with a D/max-2400 diffractometer (Rigaku, Japan) using Cu-Kα radiation. The surface morphologies were analyzed by scanning electron microscopy (SEM; FEI Quanta 250). Transmission electron microscopy (TEM) images were collected with a Philips Tecnai 12 microscope. Atomic force microscopy (AFM) measurements were performed with a Bruker Dimension Icon atomic force microscope. X-ray photoelectron spectroscopy (XPS) measurements were carried out to investigate the surface chemical compositions and states with Al Kα X-ray ($h\nu$ = 1486.6 eV) radiation (K-Alpha, Thermo Electron, USA). UV-vis diffuse reflectance spectra were obtained on a UV-vis spectrophotometer (Shimadzu, UV-2600). The electrochemical impedance spectroscopy (EIS) spectra and Mott–Schottky plots of the as-prepared thin films were measured on an electrochemical analyzer (CHI660E); the details are described in the ESI.†

Scheme 1 Schematic illustration of the preparation process of Pt–Ag/WO_3 thin films.

2.3 Photocatalytic tests

According to the test method of photocatalytic materials for the purification of water solution (GB/T 23762-2009, China), the visible light photocatalytic activities of the as-prepared samples were evaluated by the degradation of methylene blue (MB) in aqueous solution. In a typical photocatalytic experiment, the as-prepared thin-film sample using ITO glass as a substrate was fixed in the quartz frame and submerged in MB solution (5 mg L^{-1}, 100 mL). Before irradiation, the solution was magnetically stirred for 40 min in the dark to ensure the establishment of adsorption–desorption equilibrium. A 350 W Xe lamp with a cutoff filter of 420 nm was employed as the visible-light irradiation source and positioned 10 cm away from the reactor. After the light was turned on, at given time intervals (20 min), approximately 4 mL of clear MB solution was withdrawn and analyzed by recording the maximum absorbance at 664 nm in the UV-visible spectrum of MB. The percentage of degradation was calculated by C/C_0, where C is the concentration of remaining MB solution at each irradiated time interval, and C_0 is the initial concentration.

The photocatalytic stability of the Pt–Ag/WO_3 thin film was investigated by using the film in multiple cycles of the photocatalytic degradation of MB. After one cycle, the photocatalyst was filtrated and washed thoroughly with deionized water, and fresh MB solution (5 mg L^{-1}) was then added to the photocatalyst to begin the next cycle. Five consecutive cycles were completed, and each cycle lasted for 120 min.

Active-species capture experiments were carried out to study the photocatalytic mechanism. Different radical scavengers such as ethylene diamine tetraacetic acid disodium salt (EDTA–2Na, 1 mmol L^{-1}), *tert*-butyl alcohol (*t*-BuOH, 1 mmol L^{-1}) and 1,4-benzoquinone (BQ, 1 mmol L^{-1}) were added to the MB aqueous solution. The remaining experimental processes were similar to the above photocatalytic test.

3. Results and discussion

For sake of the thermal annealing process of the precursor gel, the TG/DSC curves of the precursor gel of Pt–Ag/WO_3 were examined (Fig. 1). Weight loss was observed in four consecutive steps. The first step of mass loss (7.6%) occurred between 30 °C and 210 °C with an endothermic peak at 102 °C and was due to the loss of surface water and dehydration. The second stage of mass loss (8.1%) occurred between 210 °C and 270 °C with an exothermic band centered at 237 °C; this may have been due to the thermal evaporation and decomposition of HCl, NO_3^-, and other species from the raw material. The decomposition process of the film started from at 270 °C and proceeded until 470 °C in two consecutive steps, with mass losses of 4.2% and 5.2% corresponding to the third and fourth stages, respectively. An exothermic peak was observed at 446 °C, which can be attributed to the thermal decomposition of PVA.[29] At temperatures above 470 °C, the residual weight remains constant, and the final exothermic peak at 515 °C is attributable to the transformation of the amorphous structure to the monoclinic phase of WO_3. This result implies that 550 °C is a proper calcination temperature for the formation of Pt–Ag/WO_3.
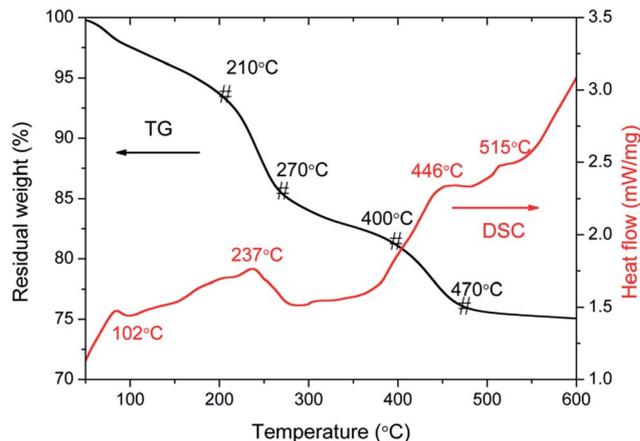

Fig. 1 TG/DSC curves of the precursor gel of Pt–Ag/WO_3.

Fig. 2 shows the XRD patterns of ITO glass and the as-prepared samples. It is clear that all of the as-prepared samples showed polycrystalline structures, and all of the peaks were attributed to the monoclinic phase of WO_3 (JCPDS 43-1035), except those attributed to ITO glass. It is noted that the peaks attributed to ITO glass were observed in the pure WO_3, Pt/WO_3, Ag/WO_3, and Pt–Ag/WO_3 films. This is because the films were relatively thin. In addition, no diffraction peaks attributed to Pt, Ag, and Pt–Ag were observed in the Pt/WO_3, Ag/WO_3, and Pt–Ag/WO_3 samples, respectively, indicating that the contents of these noble metals in the composite films were relatively low.

Fig. 3 shows the SEM images of these four samples at low magnification (8000×). The images illustrate the characteristic larger-scale microstructures of the samples. Fig. 3a shows that the pure WO_3 film is dense and composed of particles with sizes of around 500 nm. In contrast, Fig. 3b–d show completely different microstructures for the Pt/WO_3, Ag/WO_3, and Pt–Ag/WO_3 films. The Pt/WO_3 film is composed of long, flat strips and isolated islands, while the Ag/WO_3 film is composed of long, flat
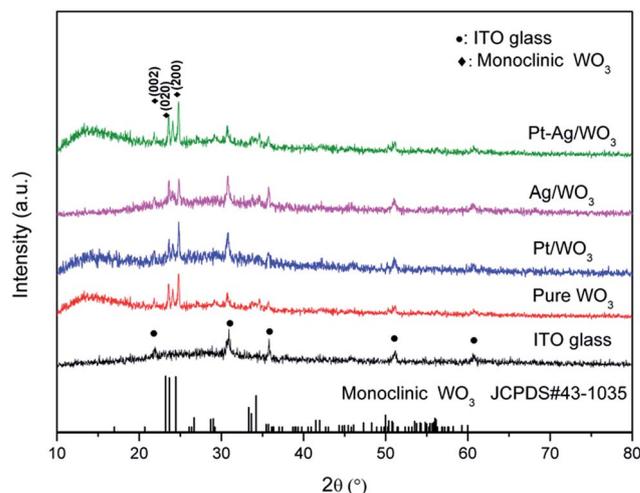

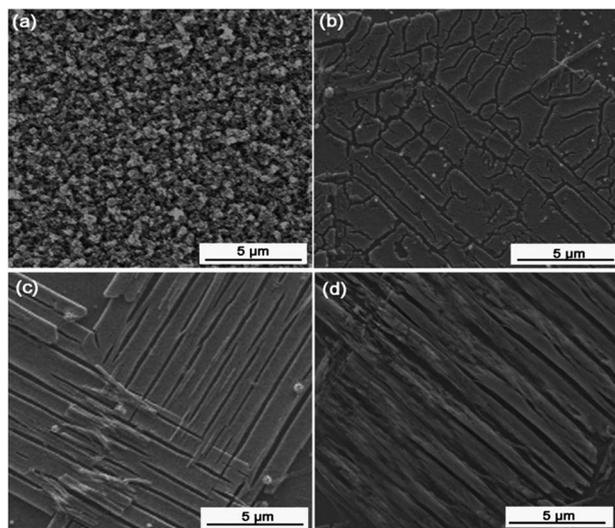Fig. 2 XRD patterns of ITO glass and the as-prepared samples.

Fig. 3 SEM images of pure WO_3 (a), Pt/WO_3 (b), Ag/WO_3 (c), and Pt–Ag/WO_3 (d) thin films.

strips with lengths of several micrometers and widths of 1 μm. In the Pt–Ag/WO_3 film, the long, flat strips were arranged along the same direction. Overall, the morphologies of the Pt/WO_3, Ag/WO_3, and Pt–Ag/WO_3 films are similar. In addition, a piece of the Pt–Ag/WO_3 thin film was peeled off from the ITO substrate and treated ultrasonically for TEM imaging. The corresponding TEM images of the Pt–Ag/WO_3 sample are shown in Fig. S1 in ESI.† It can be seen that uniform Pt–Ag nanoparticles with sizes less than 5 nm were obtained.

The microstructures of these four samples were further observed at a more local scale using AFM. The scanned areas of the AFM images were 5 μm × 5 μm. Fig. 4a shows that pure WO_3
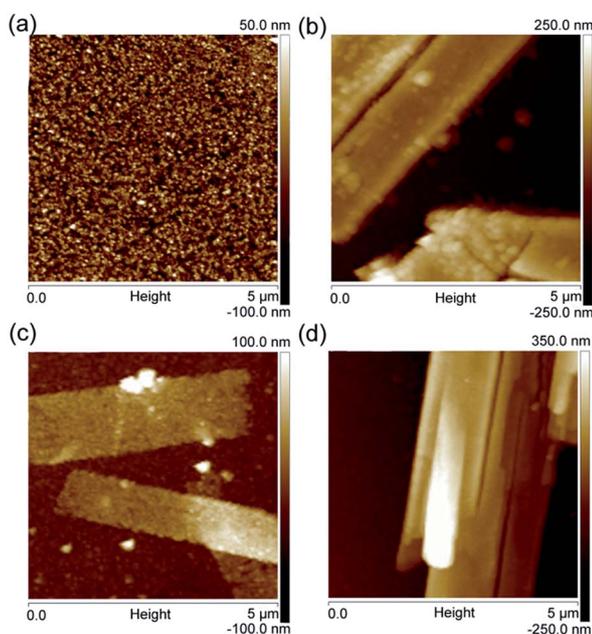

Fig. 4 AFM images of pure WO_3 (a), Pt/WO_3 (b), Ag/WO_3 (c), and Pt–Ag/WO_3 (d) thin films.

film exhibits small and uniform particle morphologies. In contrast, the Pt/WO_3, Ag/WO_3, and Pt–Ag/WO_3 films are composed of long, flat strips, as shown in Fig. 4b–d, which is consistent with the SEM results in Fig. 3.

To determine the detailed elemental compositions of the samples, the XPS survey spectra of the as-prepared pure WO_3, Pt/WO_3, Ag/WO_3 and Pt–Ag/WO_3 thin films were collected and are displayed in Fig. S2 in ESI.† It can be seen that the survey spectrum of pure WO_3 is dominated by the signals of W, O, and C (contaminant). The survey spectrum of the Pt/WO_3 film confirms the presence of W, O, C, and slight Pt. In addition, an obvious Ag signal was observed in the survey spectrum of the Ag/WO_3 sample, while slight Pt and Ag signals were found in that of the Pt–Ag/WO_3 sample. It is also noted that the signals of In and Sn were observed, which could be related to the compositions of the ITO substrates.

Fig. 5a shows the high-resolution W 4f core-level spectra of the as-prepared pure WO_3, Pt/WO_3, Ag/WO_3 and Pt–Ag/WO_3 samples. The peaks attributed to W $4f_{5/2}$ and W $4f_{7/2}$ in the spectra of the Pt/WO_3, Ag/WO_3 and Pt–Ag/WO_3 samples clearly shifted to higher binding energies compared to those in the spectrum of pure WO_3. This may have resulted from the chemical interaction between Pt, Ag, Pt–Ag and WO_3 in the samples of Pt/WO_3, Ag/WO_3 and Pt–Ag/WO_3, respectively. Fig. 5b presents the XPS spectra of Pt 4f for the Pt/WO_3 and Pt–Ag/WO_3 samples; the Pt $4f_{5/2}$ and Pt $4f_{7/2}$ peaks were located at 74.6 and 71.4 eV, respectively, indicating that Pt is mainly present in the metallic state in the Pt/WO_3 sample.[30] The peaks of Pt $4f_{7/2}$ and Pt $4f_{5/2}$ in the spectrum of the Pt–Ag/WO_3 sample were shifted to lower values by approximately 0.6–0.8 eV compared to in the spectrum of the Pt/WO_3 sample, suggesting a change in the electronic environment of Pt and a local increase in the electron density on Pt[9] in the Pt–Ag/WO_3 sample. This might originate from the chemical interaction between Pt and Ag, which decreases the binding energy when Pt atoms act as electron acceptors.[31] A similar result is shown in the XPS spectra of Ag 3d for Ag/WO_3 and Pt–Ag/WO_3 (Fig. 5c). The observation of the Ag $3d_{3/2}$ and Ag $3d_{5/2}$ peaks at 373.5 and 367.6 eV, respectively, indicates that Ag is mainly present in the metallic state in the Ag/WO_3 sample.[32] Moreover, the Ag 3d binding energy of the Pt–Ag/WO_3 sample shifted to a lower binding energy with respect to that of the Ag/WO_3 sample. This is indicative of a change in the electronic structure of Pt upon the formation of the alloy with Ag.[19] A similar result was observed in Pt–Cu bimetallic nanoassemblies.[33] Furthermore, the elemental surface compositions were determined by XPS. According to the XPS analysis, the contents of Pt and Ag in the Pt–Ag/WO_3 thin film are 0.24 and 0.48 atom%, respectively.

The UV-vis absorption spectra of these different photocatalysts are compared in Fig. 6a. All samples exhibited strong peaks below 400 nm, which are assigned to the inter-band transition of the WO_3 film.[11] The Pt/WO_3 catalyst shows increased absorbance at $\lambda > 300$ nm due to the scattering of light by the Pt particles.[34,35] The Ag/WO_3 sample shows a slightly broadened peak around 450–650 nm, which is assigned to the surface plasmon resonance effect of the metallic Ag particles.[36–38] It is also noted that the plasmon resonance absorbance
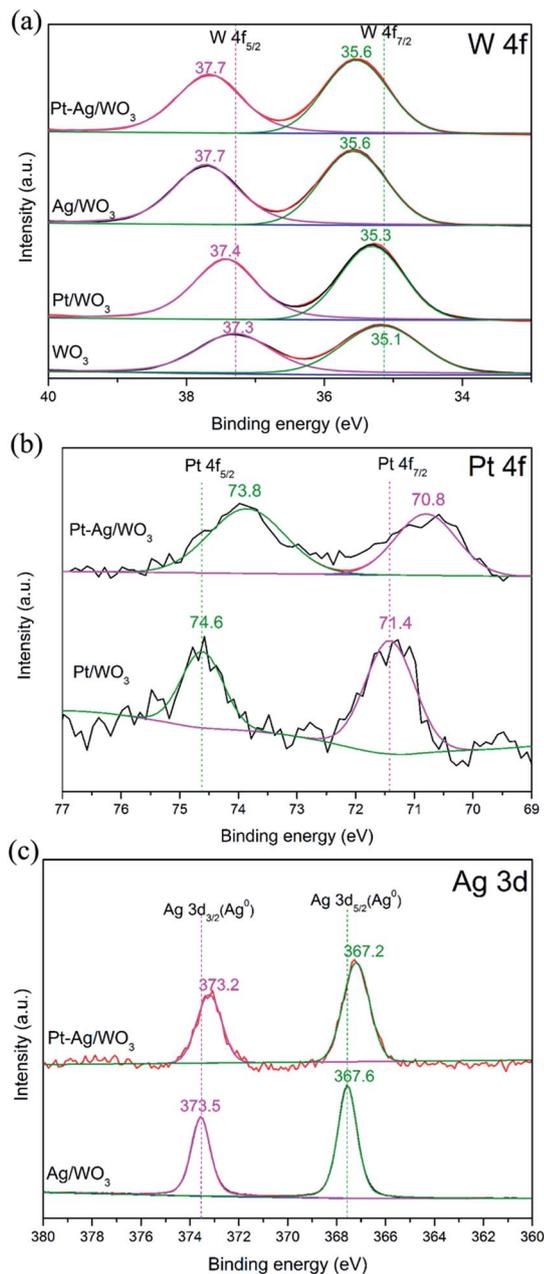
Fig. 5 XPS spectra of (a) W 4f and (b) Pt 4f and (c) Ag 3d high-resolution spectra for the different as-prepared samples.
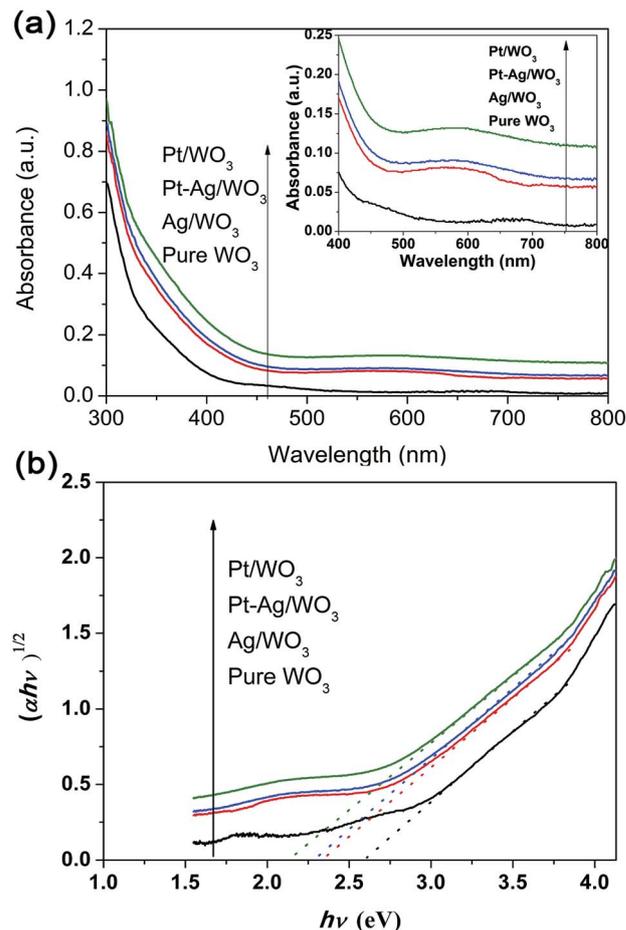

Fig. 6 (a) UV-vis diffuse reflectance absorption spectra of the as-prepared samples (the inset shows the region from 400 to 800 nm). (b) Plots of $(\alpha h\nu)^{1/2}$ versus photon energy $h\nu$ of these samples.

of Ag particles was not distinct, which might result from the low content of Ag in the Ag/WO$_3$ catalyst. Additionally, the Pt–Ag/WO$_3$ catalysts exhibit similar absorption spectra as the Ag/WO$_3$ catalyst due to the slight surface plasmon resonance effect of the metallic Ag particles. The band gap energies (E_g) of these samples were calculated from the absorption data using the following equation:

$$\alpha h\nu = A(h\nu - E_g)^n, \qquad (1)$$

where α is the absorption coefficient, A is the absorption constant, and n is a constant that depends on the probability of transition and takes values 1/2 and 2 for direct allowed and indirect allowed transitions, respectively. Because WO$_3$ has an indirect band gap, the E_g values of the samples were estimated from the intercept of the tangent in the plots of $(\alpha h\nu)^{1/2}$ versus photon energy $h\nu$ (Fig. 6b). The results show that the band gap energies (E_g) of pure WO$_3$, Ag–WO$_3$, Pt–WO$_3$ and Pt–Ag/WO$_3$ are 2.6, 2.35, 2.13, and 2.28 eV, respectively. The narrowing of the band gap energies of Ag–WO$_3$, Pt–WO$_3$ and Pt–Ag/WO$_3$ might be related to the modification of the electronic structure of WO$_3$ compared with that of pure WO$_3$, which needs deeper investigation in the future.

MB was used as a target pollutant to evaluate the photocatalytic activity of the as-prepared samples because the self-degradation of MB is negligible under visible light (see Fig. 7a). The variation in the absorption intensity of MB dye solution over pure WO$_3$, Pt/WO$_3$, Ag/WO$_3$ and Pt–Ag/WO$_3$ thin films at different irradiation times is recorded in Fig. S3 in ESI.† It can be seen that the maximum absorption of MB dye solution is at 664 nm, and the intensity of the absorption peak decreased with increasing irradiation time for each sample. Based on these changes in absorption intensity, the photocatalytic degradation ratios of MB solution in the presence of pure WO$_3$, Pt/WO$_3$, Ag/WO$_3$ and Pt–Ag/WO$_3$ thin films are expressed in Fig. 7a. It can be seen that the photocatalytic degradation
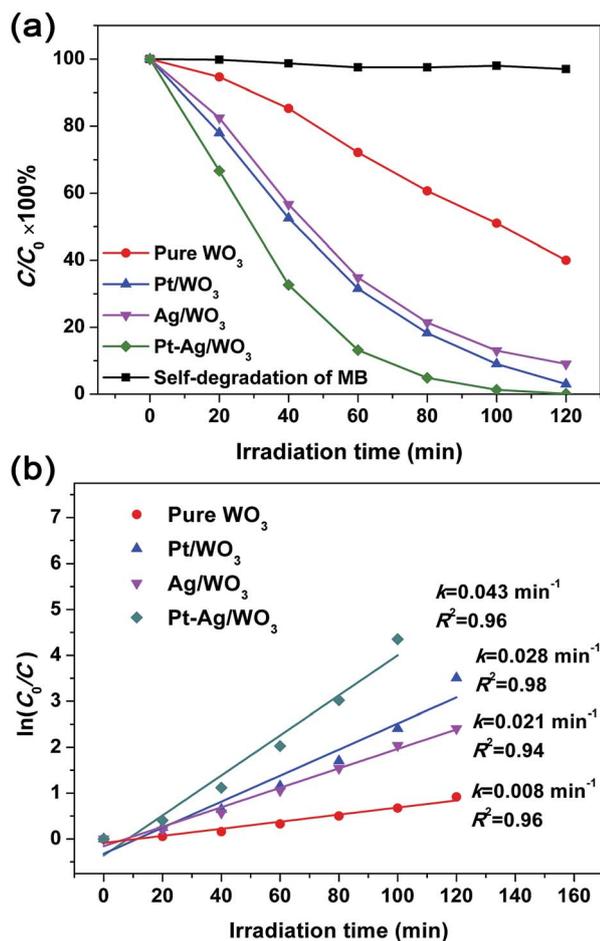
Fig. 7 (a) Photocatalytic degradation ratio of MB solution in the presence of pure WO_3, Pt/WO_3, Ag/WO_3 and $Pt–Ag/WO_3$ thin films. (b) Plots of $\ln(C_0/C)$ versus irradiation time.

efficiency follows the order: $Pt–Ag/WO_3 > Pt/WO_3 > Ag/WO_3 >$ pure WO_3. It is clear that the $Pt–Ag/WO_3$ thin film shows the best photocatalytic activity. About 98% of the initial MB decomposed after 120 min in the presence of the $Pt–Ag/WO_3$ thin film, whereas ~60% of the dye molecules were decomposed over the pure WO_3 thin film after the same time period. In addition, about 95% and 90% of the initial MB molecules were decomposed by Pt/WO_3 and Ag/WO_3 thin films after 120 min, respectively. Although the concentration of MB was low (5 mg L^{-1}), a long irradiation time (nearly 120 min) was needed for the complete degradation of MB in the presence of the $Pt–Ag/WO_3$ thin film. This is because the thin-film photocatalyst is deposited on a substrate, leading to a significant decrease in the absorption of light and contact with pollutant molecules. Therefore, the photocatalytic activities of thin films are often lower than those of powder photocatalysts. However, thin-film photocatalysts can be repeatedly used without complicated recycling processes, which are required for conventional powder photocatalysts, and are hardly lost during photocatalytic reactions; these are the main advantages of thin-film photocatalysts.

The degradation of dyes was reported to proceed via a pseudo-first order reaction with a Langmuir–Hinshelwood

model when the initial concentration (C_0) of the dye solution is small:[39]

$$\ln(C_0/C) = kt, \qquad (2)$$

where C_0 and C are the initial concentration and remaining concentration of MB solution, respectively, k is the first-order reaction rate constant, and t is the irradiation time. In our case, the initial concentration of MB is relatively small (5 mg L^{-1}); thus, the Langmuir–Hinshelwood model was applied to estimate the first-order reaction rate constant. Fig. 7b displays the plots of $\ln(C_0/C)$ versus irradiation time. Higher slope indicates a faster degradation rate of MB solution. It is found that the reaction rate constant of the $Pt–Ag/WO_3$ thin film is about five times greater than that of the pure WO_3 thin film. In addition, the correlation coefficient (R^2) represents the relevance between practical photocatalytic reaction and linear fit.[40] The R^2 values of the as-prepared samples are above 0.9, suggesting that the data fit the first-order kinetic model well.

To investigate the photocatalytic stability of the $Pt–Ag/WO_3$ thin film, cycling runs for the photocatalytic degradation of MB was carried out, and the results are displayed in Fig. 8. It is found that the $Pt–Ag/WO_3$ thin film maintains a high photocatalytic degradation ratio (above 90%), even after five cycles. This result clearly indicates that the $Pt–Ag/WO_3$ thin film possesses excellent photocatalytic stability for MB degradation.

EIS analysis is a powerful tool for studying the charge-transfer processes. The EIS Nyquist plots of the four samples are shown in Fig. 9a. It is clear that the $Pt–Ag/WO_3$ film showed a smaller semicircle than the pure WO_3, Pt/WO_3 and Ag/WO_3 electrodes, indicating that the introduction of Pt–Ag alloy nanoparticles greatly benefited charge transfer; that is, Pt–Ag alloy nanoparticles were more effective in trapping the electrons from the CB of WO_3. Mott–Schottky experiments were carried out using the pure WO_3, Pt/WO_3, Ag/WO_3, and $Pt–Ag/WO_3$ thin-film electrodes (Fig. 9b). All four samples showed positive slopes in the Mott–Schottky plots, indicating that the as-prepared pure WO_3, Pt/WO_3, Ag/WO_3, and $Pt–Ag/WO_3$ films
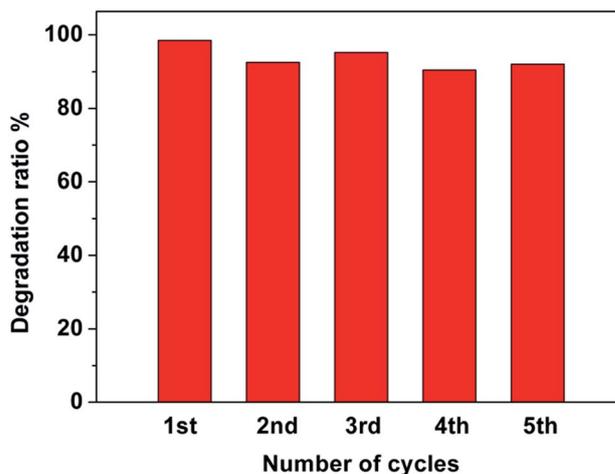

Fig. 8 Recycling experiments towards MB degradation over Pt–Ag/WO_3 thin film.
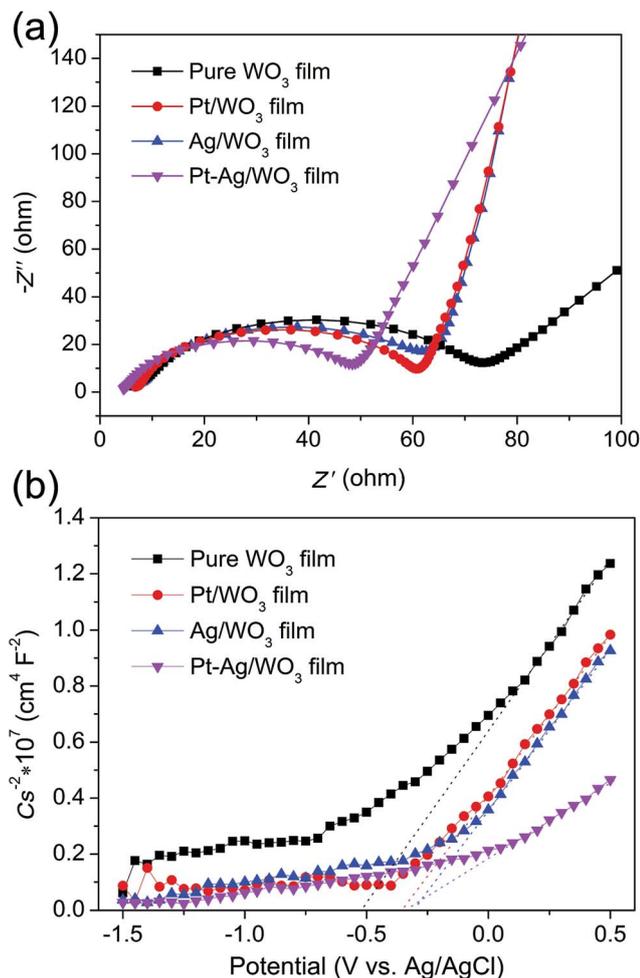
Fig. 9 EIS Nyquist plots (a) and Mott–Schottky plots (b) of the pure WO₃, Pt/WO₃, Ag/WO₃, and Pt–Ag/WO₃ thin-film electrodes.

are n-type semiconductors. Importantly, the Pt–Ag/WO₃ film sample exhibited the smallest slope in the Mott–Schottky plot, suggesting that the photogenerated electrons had the fastest charge-transfer rate.[41] These results further confirm that compared with the pure WO₃, Pt/WO₃, and Ag/WO₃ films, the Pt–Ag/WO₃ film better promotes charge transfer and thus significantly enhances the photocatalytic activity.

For a photocatalytic reaction, it is necessary to ensure that active species are generated during the photo-degradation process. It is known that the active species can be identified by free radical- and hole-trapping experiments. In our case, BQ, EDTA–2Na, and t-BuOH were used as the superoxide radical ($\cdot O_2^-$) scavenger, hole (h⁺) scavenger, and hydroxyl radical ($\cdot OH$) scavenger, respectively.[42–44] Fig. 10 shows the influence of the different scavengers on the visible-light photocatalytic activity of the Pt–Ag/WO₃ thin film toward MB degradation. Compared with the Pt–Ag/WO₃ system without scavenger, the degradation rate of MB is hardly inhibited after the addition of BQ (1 mM) in the reaction system. In contrast, in the presence of EDTA–2Na (1 mM), the degradation rate of MB is obviously decreased. Moreover, the photocatalytic activity of the Pt–Ag/WO₃ film was greatly decreased by the addition of t-BuOH.
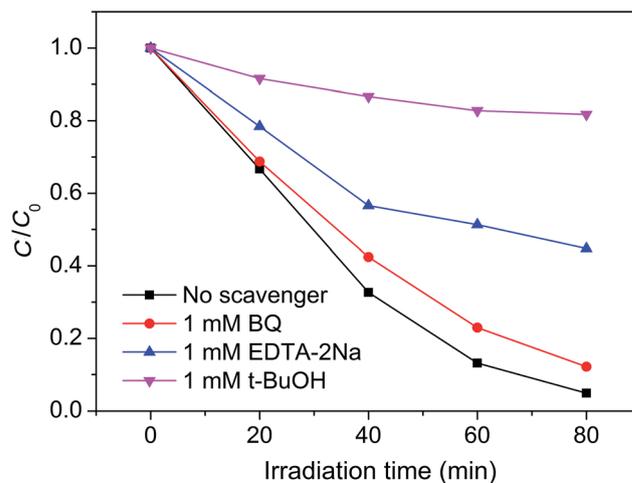

Fig. 10 Plots of photogenerated carrier trapping during the photo-degradation of MB by Pt–Ag/WO₃ thin film under visible-light irradiation.

These results indicate that h⁺ is one of the active species, while $\cdot OH$ is the main active species responsible for the oxidization of MB under visible-light irradiation. As for $\cdot O_2^-$, it is hardly generated in the Pt–Ag/WO₃ photocatalytic system.

Investigations on the enhanced photocatalytic mechanism are necessary to understand the enhanced photocatalytic activity. Here, we discuss it in detail based on the band structure and work functions. It was reported that the work functions (Φ) of WO₃ film, metallic Pt, and metallic Ag are 5.7 eV,[45–47] 5.65 eV,[48] and 4.26 eV,[49] respectively. In addition, the work function of the bimetallic alloy can be expressed by the sum of the work functions of the two metal components,[50] which means that the work function of the alloy lies at a level intermediate between monometallic Pt and Ag (4.26 eV < Φ_{Pt-Ag} < 5.65 eV). If Pt, Ag or Pt–Ag contacts WO₃, the electrons will migrate from Pt or Ag or Pt–Ag to the CB of WO₃ to achieve Fermi level equilibration. As a result, the surface of WO₃ accumulates excess electrons, while Pt or Ag or Pt–Ag exhibits excess positive charge, and a deflexed energy band forms at the Pt/WO₃, Ag/WO₃ or Pt–Ag/WO₃ interface. As shown in Scheme 2a–c, the difference between the work functions of WO₃ and noble metal ($\Phi_{WO_3}-\Phi_M$) at the Pt/WO₃, Ag/WO₃ or Pt–Ag/WO₃ junction is determined to be only about 0.05 eV, 1.44 eV, and 0.05–1.44 eV, respectively. When WO₃ catalysts are illuminated under visible light, photo-generated electrons (e⁻) in the valence band (VB) of WO₃ can be excited to the CB; simultaneously, the same amount of holes (h⁺) are generated in the VB. Moreover, the deflexed energy band in the space charge region facilitates the rapid transfer of the as-excited electrons from WO₃ to Pt or Ag or Pt–Ag nanoparticles, which decreases the recombination of the photogenerated electron–hole pairs. In the Pt/WO₃ and Ag/WO₃ samples, since WO₃ has a low CB level (+0.5 V vs. NHE) that is more positive than the potential for the single-electron reduction of oxygen,[8] electrons accumulated at Pt or Ag nanoparticles may be transferred to surface-adsorbed oxygen molecules to form H_2O_2 via the multi-electron reduction of O₂.[16] In the Pt–Ag/
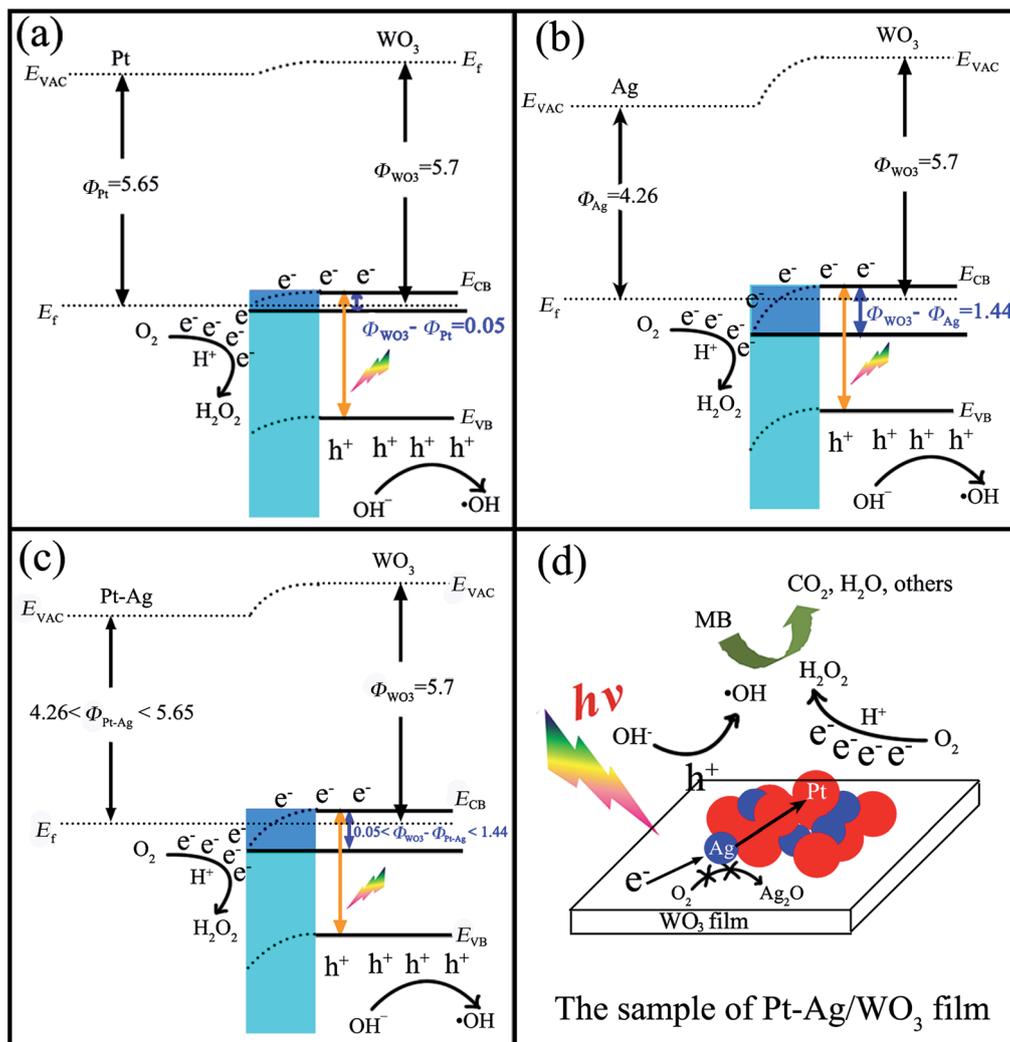
Scheme 2 Schematic energy-band diagrams for (a) Pt/WO₃, (b) Ag/WO₃, and (c) Pt–Ag/WO₃ (E_{vac}, E_{CB}, E_{VB}, E_f, Φ_M and Φ_{WO_3} denote vacuum level, Fermi level, conduction band level, valence band level, work function of metal, and work function of WO₃, respectively (in eV)). (d) Photocatalytic mechanism for the degradation of MB on the Pt–Ag/WO₃ catalyst.

WO₃ sample, an electron donation from Ag to Pt could occur because Pt (2.28) is more electronegative than Ag (1.93), leading to an increase in the electron density of Pt atoms. That is to say, the photogenerated electron from the CB of WO₃ could first transfer to Ag and then to Pt, promoting the efficient two-electron reduction of O₂ in the Pt–Ag/WO₃ sample compared to in the Pt/WO₃ and Ag/WO₃ samples, as shown in Scheme 2d. Moreover, this process leads to the two-electron reduction of O₂ occurring on the surface of Pt instead of Ag, preventing contact between Ag and O₂ and thus avoiding the oxidation of Ag in the Pt–Ag/WO₃ sample during photodegradation in air. These alloying effects result in the increased formation of H₂O₂ on the Pt–Ag/WO₃ catalyst, similar to in a Au–Ag/TiO₂ catalyst.[51] On the other hand, the leaving h⁺ with high oxidation potential (+3 V vs. NHE)[52] are apt to react with surface-bound H₂O or OH⁻ to produce ˙OH, which is consistent with the results of the photogenerated carrier-trapping experiment (Fig. 10). Additionally, it was reported that H₂O₂ can degrade dye molecules.[6] As a result, the adsorbed MB molecules can be effectively degraded

by these reactive oxidative species, including ˙OH and H₂O₂, over the Pt–Ag/WO₃ film photocatalyst under visible-light irradiation.

4. Conclusions

In this work, Pt/WO₃, Ag/WO₃, and Pt–Ag/WO₃ thin films were successfully synthesized by a three-step method involving the formation of a homogeneous precursor sol, spin coating as well as UV-light reduction, and calcination. The as-prepared Pt/WO₃, Ag/WO₃, and Pt–Ag/WO₃ thin films showed similar morphologies mainly composed of long, flat strips. The XPS results suggested a change in the electronic structure of Pt upon alloying with Ag. Moreover, the EIS and MS plots demonstrated that the Pt–Ag/WO₃ thin film can promote charge transfer and thus significantly enhance the photocatalytic activity compared with the Pt/WO₃ and Ag/WO₃ thin films. Active species-capture experiments indicated that ˙OH was the main active species responsible for the oxidization of MB. What's more, the

photogenerated electrons from the CB of WO_3 could first transfer to Ag and then to Pt, promoting the efficient two-electron reduction of O_2 in the Pt–Ag/WO_3 sample compared to in the Pt/WO_3 and Ag/WO_3 samples. Additionally, the effects of Pt–Ag alloy nanoparticles on the photocatalytic activity of WO_3 thin film are significant, and corresponding investigations of this subject are in progress.

Acknowledgements

Notes and references

1 K. Hashimoto, H. Irie and A. Fujishima, *Jpn. J. Appl. Phys.*, 2005, **44**, 8269.
2 K. Nakata and A. Fujishima, *J. Photochem. Photobiol., C*, 2012, **13**, 169–189.
3 C. Janáky, K. Rajeshwar, N. De Tacconi, W. Chanmanee and M. Huda, *Catal. Today*, 2013, **199**, 53–64.
4 G. R. Bamwenda and H. Arakawa, *Appl. Catal., A*, 2001, **210**, 181–191.
5 K. Sayama, H. Hayashi, T. Arai, M. Yanagida, T. Gunji and H. Sugihara, *Appl. Catal., B*, 2010, **94**, 150–157.
6 B. Weng, J. Wu, N. Zhang and Y.-J. Xu, *Langmuir*, 2014, **30**, 5574–5584.
7 A. Tanaka, K. Hashimoto and H. Kominami, *J. Am. Chem. Soc.*, 2014, **136**, 586–589.
8 R. Abe, H. Takami, N. Murakami and B. Ohtani, *J. Am. Chem. Soc.*, 2008, **130**, 7780–7781.
9 J. Wang, Z. Wang and C.-J. Liu, *ACS Appl. Mater. Interfaces*, 2014, **6**, 12860–12867.
10 Y. Shiraishi, Y. Sugano, S. Ichikawa and T. Hirai, *Catal. Sci. Technol.*, 2012, **2**, 400–405.
11 M. Miyauchi, *Phys. Chem. Chem. Phys.*, 2008, **10**, 6258–6265.
12 A. Fujii, Z. Meng, C. Yogi, T. Hashishin, T. Sanada and K. Kojima, *Surf. Coat. Technol.*, 2015, **271**, 251–258.
13 T. Ohashi, T. Sugimoto, K. Sako, S. Hayakawa, K. Katagiri and K. Inumaru, *Catal. Sci. Technol.*, 2015, **5**, 1163–1168.
14 G. Xi, J. Ye, Q. Ma, N. Su, H. Bai and C. Wang, *J. Am. Chem. Soc.*, 2012, **134**, 6508–6511.
15 P. Dong, N. Xu, Y. Xu and X. Wang, *Catal. Commun.*, 2016, **84**, 142–146.
16 S. Sun, W. Wang, S. Zeng, M. Shang and L. Zhang, *J. Hazard. Mater.*, 2010, **178**, 427–433.
17 W. He, X. Wu, J. Liu, K. Zhang, W. Chu, L. Feng, X. Hu, W. Zhou and S. Xie, *J. Phys. Chem. C*, 2009, **113**, 10505–10510.
18 K. Kim, K. L. Kim and K. S. Shin, *J. Phys. Chem. C*, 2011, **115**, 23374–23380.
19 J. Xu, T. Zhao and Z. Liang, *J. Phys. Chem. C*, 2008, **112**, 17362–17367.
20 Z. Jiao, J. Wang, L. Ke, X. W. Sun and H. V. Demir, *ACS Appl. Mater. Interfaces*, 2011, **3**, 229–236.
21 S. H. Baeck, K. S. Choi, T. F. Jaramillo, G. D. Stucky and E. W. McFarland, *Adv. Mater.*, 2003, **15**, 1269–1273.
22 N. Oka, A. Murata, S.-i. Nakamura, J. Jia, Y. Iwabuchi, H. Kotsubo and Y. Shigesato, *APL Mater.*, 2015, **3**, 104407.
23 M. Choobtashani and O. Akhavan, *Appl. Surf. Sci.*, 2013, **276**, 628–634.
24 H. Katsumata, K. Inoue, T. Suzuki and S. Kaneco, *Catal. Lett.*, 2014, **144**, 837–842.
25 J. Y. Zheng, G. Song, J. Hong, T. K. Van, A. U. Pawar, D. Y. Kim, C. W. Kim, Z. Haider and Y. S. Kang, *Cryst. Growth Des.*, 2014, **14**, 6057–6066.
26 D. Vernardou, H. Drosos, E. Spanakis, E. Koudoumas, C. Savvakis and N. Katsarakis, *J. Mater. Chem.*, 2011, **21**, 513–517.
27 A. Srinivasan and M. Miyauchi, *J. Phys. Chem. C*, 2012, **116**, 15421–15426.
28 G. Leftheriotis, M. Liveri, M. Galanopoulou, I. D. Manariotis and P. Yianoulis, *Thin Solid Films*, 2014, **573**, 6–13.
29 V. A. Pereira Jr, I. N. Q. de Arruda and R. Stefani, *Food Hydrocolloids*, 2015, **43**, 180–188.
30 G. P. Jin, X. Peng, Y. F. Ding, W. Q. Liu and J. M. Ye, *J. Solid State Electrochem.*, 2009, **13**, 967–973.
31 L. Qiu, F. Liu, L. Zhao, W. Yang and J. Yao, *Langmuir*, 2006, **22**, 4480–4482.
32 Z. Jiang and J. Xie, *RSC Adv.*, 2015, **6**, 3186–3197.
33 G. Fu, H. Liu, N. You, J. Wu, D. Sun, L. Xu, Y. Tang and Y. Chen, *Nano Res.*, 2016, **9**, 755–765.
34 Y. Shiraishi, Y. Sugano, S. Tanaka and T. Hirai, *Angew. Chem.*, 2010, **122**, 1700–1704.
35 Y. Shiraishi, Y. Takeda, Y. Sugano, S. Ichikawa, S. Tanaka and T. Hirai, *Chem. Commun.*, 2011, **47**, 7863–7865.
36 H. M. Coleman, K. Chiang and R. Amal, *Chem.–Eur. J.*, 2005, **113**, 65–72.
37 H. Zhang, G. Wang, D. Chen, X. Lv and J. Li, *Chem. Mater.*, 2008, **20**, 6543–6549.
38 Y. Han, J. Zhou, W. Wang, H. Wan, Z. Xu, S. Zheng and D. Zhu, *Appl. Catal., B*, 2012, **125**, 172–179.
39 X. Wang, J.-G. Li, H. Kamiyama, Y. Moriyoshi and T. Ishigaki, *J. Phys. Chem. B*, 2006, **110**, 6804–6809.
40 P. Dong, Y. Wang, H. Li, H. Li, X. Ma and L. Han, *J. Mater. Chem. A*, 2013, **1**, 4651–4656.
41 F. Su, T. Wang, R. Lv, J. Zhang, P. Zhang, J. Lu and J. Gong, *Nanoscale*, 2013, **5**, 9001–9009.
42 C. Chen, Q. Wang, P. Lei, W. Song, W. Ma and J. Zhao, *Environ. Sci. Technol.*, 2006, **40**, 3965–3970.
43 C. Pan and Y. Zhu, *Environ. Sci. Technol.*, 2010, **44**, 5570–5574.
44 H. Lee and W. Choi, *Environ. Sci. Technol.*, 2002, **36**, 3872–3878.
45 G. Vida, V. Josepovits, M. Gyor and P. Deak, *Microsc. Microanal.*, 2003, **9**, 337–342.

46 A. Yella, U. K. Gautam, E. Mugnaioli, M. Panthöfer, Y. Bando, D. Golberg, U. Kolb and W. Tremel, *CrystEngComm*, 2011, **13**, 4074–4081.

47 K. Cheng, Z. Qiao, S. Pang, S. Wang, X. Han and Z. Du, *Appl. Phys. Express*, 2012, **5**, 105801–105803.

48 H. B. Michaelson, *J. Appl. Phys.*, 1977, **48**, 4729–4733.

49 C.-M. Chen, C.-M. Liu, K.-H. Wei, U. S. Jeng and C.-H. Su, *J. Mater. Chem.*, 2012, **22**, 454–461.

50 R. Ishii, K. Matsumura, A. Sakai and T. Sakata, *Appl. Surf. Sci.*, 2001, **169–170**, 658–661.

51 D. Tsukamoto, A. Shiro, Y. Shiraishi, Y. Sugano, S. Ichikawa, S. Tanaka and T. Hirai, *ACS Catal.*, 2012, **2**, 599–603.

52 T. Arai, M. Yanagida, Y. Konishi, Y. Iwasaki, H. Sugihara and K. Sayama, *J. Phys. Chem. C*, 2007, **111**, 7574–7577.